Smart Structures and Systems, *Vol. 31*, *No. 2* (*2023*) *101-111*
https://doi.org/10.12989/sss.2023.31.2.101

Accuracy and robustness of hysteresis loop analysis in the identification and monitoring of plastic stiffness for highly nonlinear pinching structures

Hamish Tomlinson [1], Geoffrey W. Rodgers [1], Chao Xu [1,2], Virginie Avot [1], Cong Zhou [1,3] and J. Geoffrey Chase*[1]

[1] *Department of Mechanical Engineering, University of Canterbury, Private Bag 4800, Christchurch, New Zealand*
[2] *Department of Astronautics, Northwestern Polytechnical University, Xi'an, China*
[3] *Department of Civil Aviation, Yangtze River Delta Research Institute, Northwestern Polytechnical University - Taicang, Taicang, China*

(*Received December 30, 2020, Revised December 18, 2021, Accepted September 22, 2022*)

Abstract. Structural health monitoring (SHM) covers a range of damage detection strategies for buildings. In real-time, SHM provides a basis for rapid decision making to optimise the speed and economic efficiency of post-event response. Previous work introduced an SHM method based on identifying structural nonlinear hysteretic parameters and their evolution from structural force-deformation hysteresis loops in real-time. This research extends and generalises this method to investigate the impact of a wide range of flag-shaped or pinching shape nonlinear hysteretic response and its impact on the SHM accuracy. A particular focus is plastic stiffness (k_p), where accurate identification of this parameter enables accurate identification of net and total plastic deformation and plastic energy dissipated, all of which are directly related to damage and infrequently assessed in SHM. A sensitivity study using a realistic seismic case study with known ground truth values investigates the impact of hysteresis loop shape, as well as added noise, on SHM accuracy using a suite of 20 ground motions from the PEER database. Monte Carlo analysis over 22,000 simulations with different hysteresis loops and added noise resulted in absolute percentage identification error (median, (IQR)) in k_p of 1.88% (0.79, 4.94)%. Errors were larger where five events (Earthquakes #1, 6, 9, 14) have very large errors over 100% for resulted k_p as an almost entirely linear response yielded only negligible plastic response, increasing identification error. The sensitivity analysis shows accuracy is reduces to within 3% when plastic drift is induced. This method shows clear potential to provide accurate, real-time metrics of non-linear stiffness and deformation to assist rapid damage assessment and decision making, utilising algorithms significantly simpler than previous non-linear structural model-based parameter identification SHM methods.

Keywords: least squares linear regression; physical parameters identification; seismic response; structural health monitoring; structural hysteresis; structural pinching

1. Introduction

Many regions are subject to seismic risk. Modern building codes demand structures remain standing, albeit with varying degrees of damage, and key structures, such as hospitals, remain in use. The ability to robustly and rapidly evaluate damage post-event is necessary, so critical decisions can be made concerning re-entry, use, and/or demolition. Damage detection strategies for buildings are called structural health monitoring (SHM) (Sohn *et al*. 2004, Doebling *et al*. 1996, Fan and Qiao 2011, Brownjohn 2007, Ye *et al*. 2014), and typically evaluate structural condition against a baseline state to detect the location and severity of damage (Doherty 1987, Doebling *et al*. 1996, Fan and Qiao 2011). Real-time or near real-time SHM is a major goal to enhance response, where many current methods require human intervention and/or post-processing (Hannan *et al*. 2018).

There are many vibration-based SHM methods based, primarily focused on modal parameter damage detection, but also including a range of Kalman filtering, Bayesian, and emerging machine learning techniques to identify parameters (e.g., Doebling *et al*. 1996, Yang *et al*. 2006, 2007, Bernal and Gunes 2000, Pan *et al*. 2016, Ye *et al*. 2017, 2019, Hannan *et al*. 2018, Sun *et al*. 2017, Xiong *et al*. 2019, Ginsberg *et al*. 2018, Brownjohn *et al*. 2019), "However, these methods are most applicable to linear structures, even when adapted to account for time-varying properties due to damage, and can be insensitive to localized damage. More importantly, nonlinear response and energy absorbing damage are potentially more critical parameters to assess safety post-event, but are not easily or directly captured with these methods (Chang *et al*. 2003).

Non-parametric methods can overcome issues with nonlinear response using statistical methods or time series analysis to identify damage (Pines and Salvino 2006, de Lautour and Omenzetter 2010, Huang *et al*. 2012, Brownjohn 2007, Brownjohn *et al*. 2019, Jesus *et al*. 2019). Neural networks and machine learning (Kao and Loh 2013, Adeli and Jiang 2006, Hung *et al*. 2003, Jiang and Adeli 2005, Wu *et al*. 2002, Ye *et al*. 2019) and ARMA (integrated

*Corresponding author, Ph.D., Professor,
E-mail: geoff.chase@canterbury.ac.nz

http://www.techno-press.org/?journal=sss&subpage=7
ISSN: 1738-1584 (Print), 1738-1991 (Online)

auto regressive moving average) models (Bao *et al*. 2013, de Lautour and Omenzetter 2010) are further examples of non-parametric SHM methods. These algorithms provide damage estimates, but can fail to generalise. Their lack of an underlying baseline model makes them unable to relate the non-parametric variables to the true physics of the structure to quantify the level of damage. Similar approaches (also) determining when damage occurred are also increasingly common, including wavelet analysis (Hou *et al*. 2000, 2006, Taha *et al*. 2006) and Hilbert-Huang transforms (Kunwar *et al*. 2013, Chen *et al*. 2014, Yang *et al*. 2004, Lin *et al*. 2005).

A major drawback of all these approaches is their inability or difficulty in sample-to-sample real-time implementation as the event occurs. In particular, for nonlinear response where parameter identification optimisation can be unreliable and optimisation may require human input, the need for accurate and rapid damage identification is greatest. With *a priori* assumption of a structural baseline model, a number of real-time SHM methods based on filtering methods have been presented to obtain time-variant model parameters (Jeen-Shang and Yigong 1994, Sato and Qi 1998, Loh *et al*. 2000, Chase *et al*. 2005, Yang *et al*. 2006). Some, in particular have addressed nonlinear hysteresis and permanent deformation (Nayyerloo *et al*. 2011, Toussi and Yao 1983, Iwan and Cifuentes 1986, Zhou *et al*. 2015a, b, 2015c, 2017a, c). However, none of these methods estimates or identifies an accurate nonlinear or plastic stiffness nor its evolution over time, which is critical to assessing major damage.

In particular, nonlinear hysteretic behaviour plays a crucial role in seismic performance-based analysis and designs (Christopoulos *et al*. 2003, Pampanin *et al*. 2003), and captures nonlinear yielding and energy absorption arising from damage (Stephens and Yao 1987). Modern sensors make it possible to generate inter-story restoring force-deformation hysteresis loops in real-time (Iemura and Jennings 1974, Iwan and Cifuentes 1986, Toussi and Yao 1983), enabling development of non-linear hysteresis-based SHM methods. The recently proposed hysteresis loop analysis (HLA) method thus identifies the time-varying evolution of nonlinear structural parameters, including equivalent linear stiffness, linear elastic stiffness, post-yielding stiffness, yield deformation, permanent deformation, and cumulative plastic deformation (Xu *et al*. 2014, Zhou *et al*. 2015a, b, c, 2017a, c).

Further, there are specific, highly nonlinear behaviours which are not well-addressed in the SHM community, but are common in reinforced concrete structures (Baber and Noori 1985, Foliente and Noori 1996, Sivaselvan and Reinhorn 2000, Yu *et al*. 2016, Favvata and Karayannis 2014). They are emerging due to the increasing use of self-centring systems (Christopoulos *et al*. 2008, Ozbulut and Hurlebaus, 2010, Tremblay *et al*. 2008, Attanasi *et al*. 2009, Rodgers *et al*. 2008, 2011, 2012, Wrzesniak *et al*. 2016). While well-modeled (Baber and Noori 1985, Foliente and Noori 1996, Sivaselvan and Reinhorn 2000, Yu *et al*. 2016, Favvata and Karayannis 2014), pinching is less-studied in SHM due to its nonlinearity (Wu and Smyth 2008, Kunnath *et al*. 1997, Yang *et al*. 2014), and these studies only assess degradation, but not specific stiffness values nor nonlinear stiffness changes and evolution.

The specific novelty of this study is in extending and generalising the HLA method by fully assessing its robustness to hysteresis loop shape, including time-varying pinching or flag-shaped behaviour. The examination of highly nonlinear flag-shaped and pinching behaviours, which are not well-studied in SHM, as well as other loop shapes, is important because any realistic SHM algorithm should be general to all possible response types. More specifically, generalisability and robustness of the HLA method is assessed, which is critical to ensure all degradation is both accurately identified and thus accurately tracked. This study focuses in particular on plastic stiffness (k_p), where accurate identification of this parameter enables accurate identification of net and total plastic deformation and plastic energy dissipated, all of which are directly related to damage and infrequently assessed in SHM.

2. Methods

This study focuses on identifying post-yield stiffness (k_p) over a suite of 20 earthquakes (Christopoulos *et al*. 2002, PEER 2005) for a range of hysteresis loop shapes. Post-yield stiffness is the slope of the plastic regime of the force-displacement hysteresis loop. Consistent, accurate parameter identification of plastic stiffness, in the presence of sensor noise and different ground motions, is critical to characterise a SHM algorithm's generality and robustness in quantifying plastic deformation and energy absorbed, which are often ignored key damage metrics due to the difficulty in identifying them rapidly and accurately from limited measured data.

More specifically, the ground motions are highly and broadly representative of a range of design level events. In particular, the set of records used in the analysis presented within this manuscript represent earthquake magnitudes from 6.7 to 7.3, and with epicentral distances from 13.7 to 25.8 km, and different recording site soil classes. This suite of records represents a relatively wide range of conditions for recording of ground motions. While these records date back to a study from 2005, it is expected those ground motion records remain representative of ground motions those which might be experienced today, as geological conditions and seismic sensing technology have not changed significantly in the intervening period. Hence, the results provided using this suite, scaled to similar levels with a wide range of characteristics, should be generalisable and robust, as seen in other studies using this suite of ground motions (Vamvatsikos and Cornell 2002).

2.1 Construction of hysteresis loops

Nonlinear structural load-deflection hysteresis loops contain structural performance information, such as energy dissipation, permanent deformation and structural deterioration, and can be generated from seismic response data (Iemura and Jennings 1974, Iwan and Cifuentes 1986,

Toussi and Yao 1983). A single-degree-freedom (SDOF) numerical system is used, thus assuming a typical first mode dominant seismic response, to provide a proof of concept analysis with a known ground truth. The nonlinear equation of motion is defined

$$m\ddot{x}(t) + f(x, \dot{x}) = -ma(t) \tag{1}$$

Where x , $\dot{x}$ and $\ddot{x}$ are inter-story response displacement, velocity and acceleration respectively; $f(x, \dot{x})$ is the nonlinear restoring force including damping, nonlinear elasto-plastic response and hysteresis in a flag-shaped model; $a(t)$ is ground acceleration and m is the mass. Numerical double integration of acceleration response yields inter-story displacement, assuming use of a low rate displacement sensor (Hann *et al*. 2009, Skolnik and Wallace 2010, Boore and Bommer 2005, Wu and Smyth 2008), or it can be directly measured using emerging displacement measurement methods (Xu and Brownjohn 2018, Park *et al*. 2015, Ye *et al*. 2015, Feng and Feng 2017, 2018).

A flag-shape piecewise nonlinear model is defined to represent the force-displacement relationship of hysteresis, as shown in Fig. 1. The parameters characterizing the properties of this hysteretic model are *ke*, *α*, *β* and *dy*. The coefficient *ke* is the pre-yielding stiffness, *α* is the ratio of post-yielding stiffness to pre-yielding stiffness. The energy dissipation coefficient or pinching factor *β* reflects the dissipation capacity. And *dy* is the yield displacement of the hysteresis system.

Thus, the post-yielding stiffness *kp* is defined

$$kp = \alpha \cdot ke \tag{2}$$

The flag-shaped model can be described

$$\begin{aligned} G(x) &= g_1(x) = a_1 x + b_1 X_1 \le x \le X_{t_1} \\ &= g_2(x) = a_2 x + b_2 X_{t_1} \le x \le X_{t_2} \\ &= \cdots \\ &= g_r(x) = a_r x + b_r X_{t_{r-1}} \le x \le X_n \end{aligned} \tag{3}$$

where X_{t_1},…, $X_{t_{r-1}}$ are the breakpoints in the sub-half cycles, as shown in Fig. 1(b), (X_1 , Y_1),…, (X_n , Y_n) are *n* pairs of displacement and restoring force data during the sub-half cycles, and can be represented by

$$Y_i = G(X_i) + e_i \qquad i = 1, \ldots, n \tag{4}$$

where e_i are the random errors caused by measurement noise or model uncertainty.

Therefore, the pre-yielding stiffness ke and post-yielding stiffness kp can be calculated

$$\begin{aligned} k_e &= a_1 \quad \text{for} \quad r = 1,2 \\ &= a_1 \quad \text{and} \quad a_3 \quad \text{for} \quad r = 3,4 \end{aligned} \tag{5}$$

$$\begin{aligned} k_p &= a_2 \quad \text{for} \quad r = 2,3 \\ &= a_2 \quad \text{and} \quad a_4 \quad \text{for} \quad r = 4 \end{aligned} \tag{6}$$

In addition, the pinching factor β can be described

$$\beta = \left|\frac{Y_1 - Y_{t_1}}{Y_n}\right| = \left|\frac{(a_1 X_1 + b_1) - (a_2 X_{t_1} + b_2)}{a_4 X_{t_3} + b_4}\right| \quad \text{for} \quad r = 4 \tag{7}$$

2.2 Structural pinching factor

Hysteresis loop pinching was incorporated in the model of $f(x, \dot{x})$ and the level of pinching was controlled using the pinching factor, β, in Eq. (7), which is in the range [-1, 1], where -1 represents no pinching and +1 a bilinear elasto-plastic response. It defines the fraction of the nominal yield displacement at which pinching occurs in the unloading phase of the hysteresis loop. Fig. 2 shows example loops with pinching factor -1.0, -0.5, 0, 0.5 and 1.0, respectively, with sharp elasto-plastic transitions only for clarity.

2.3 Identifying damage-based information from hysteresis loops

A structure subjected to an earthquake load may experience several inelastic deformation cycles of the general elastic-plastic form (β = -1; Fig. 2) as illustrated in Fig. 3. The elastic regime is governed by one stiffness value, k_e, and the plastic regime by a lower, k_p (Chopra 2012). For damage assessment and prediction of structural response for further analysis, it is important to obtain accurate estimates of k_e and k_p, and evolution over time

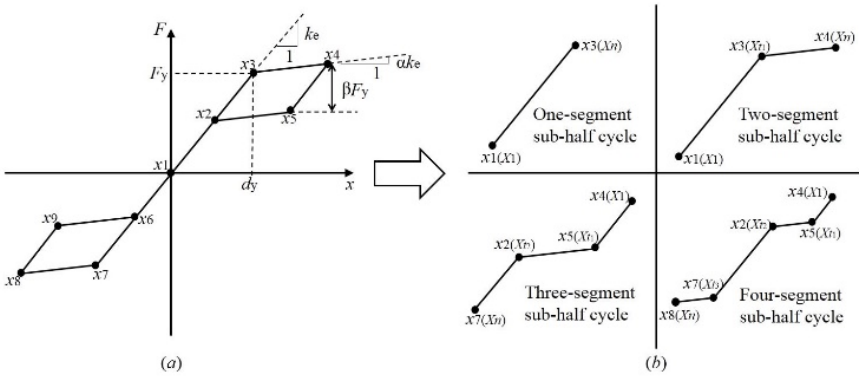

Fig. 1 (a) Flag-shaped hysteretic loop model; (b) with four types of possible half cycles for values of *r* = 1, 2, 3, and 4 in Eqs. (5)-(7)

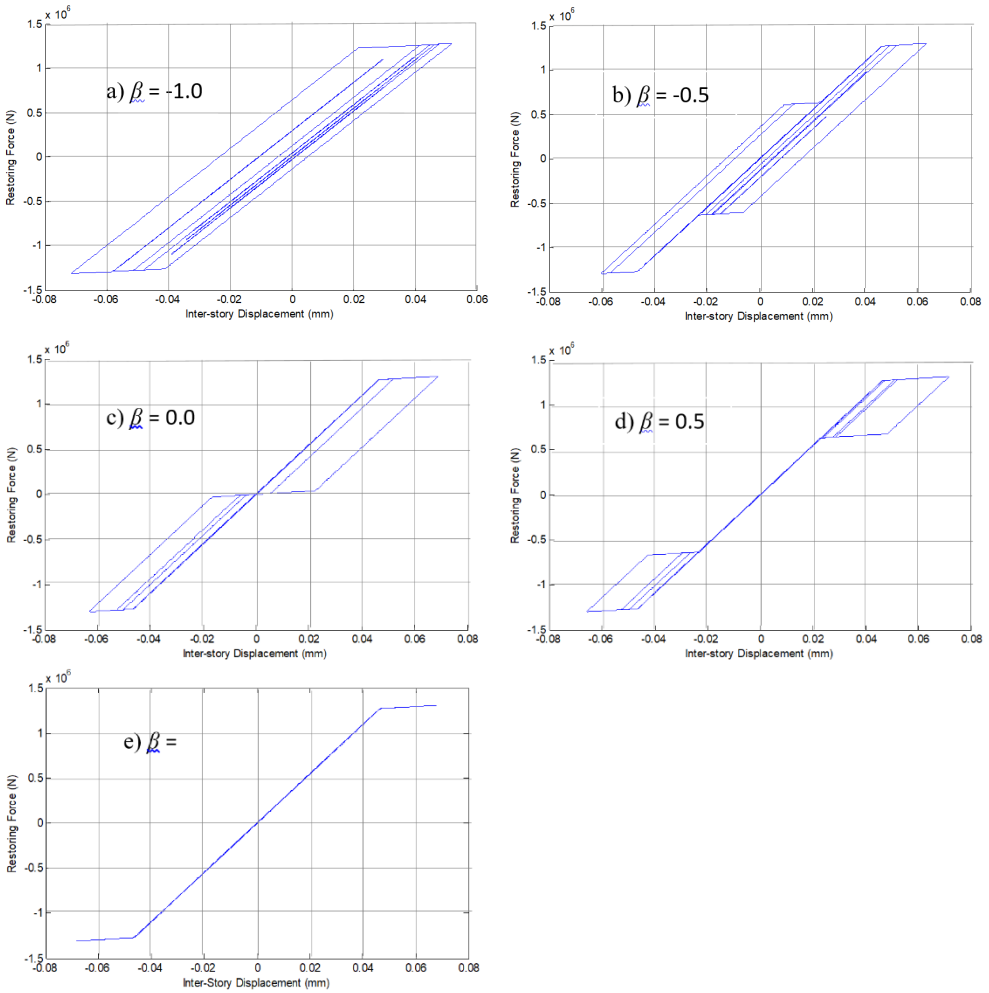

Fig. 2 Hysteresis loops generated by Eqs. (2)-(7) for a range of pinching factors, β, in Eq. (7) with sharp elasto-plastic transitions for clarity only

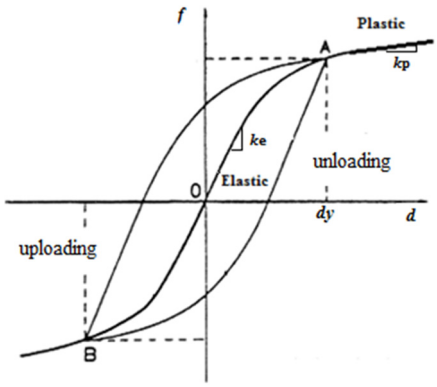

Fig. 3 General elastic-plastic behavior with β = -1 (Fig. 2) (Wen 1976)

to assess structural condition. In addition, assessing total and relative permanent deformation requires accurate estimation of k_p.

The elastic stiffness and the plastic stiffness are identified over all half cycles of structural response. A method to find the values for k_e and k_p is posed, which should be robust for all levels of pinching and thus general. First, the hysteresis loop is segmented based on positive or negative force values (segregated by the horizontal axis), "Within each section, subsections between the local maxima and minima of the resulting curve are segregated, where each subsection is a half-cycle, which is then considered individually, where Fig. 4 shows typical possible half-cycles from this model. The elastic and plastic stiffness values are identified from these half-cycles. The median elastic plastic, k_p, stiffness values is calculated. The time trajectory of these values characterises the evolution of linear and nonlinear stiffness, and thus damage, over time.

The elastic and plastic stiffness of each half-cycle is found by identifying the major turning points of the curve, and fitting a linear regression function $y = ax + b$ between these points in Fig. 4. The estimated slopes from the regression line define the elastic and plastic stiffness values. The turning points are identified as the midpoint of any major changes in the gradient of the curve. An algorithm using a statistical F-test and testing up to 4 segments per half cycle is used to decide how many lines to fit to a subsection is used, based on minimising the least squares error across all possible models in Fig. 4, and making sure no adjacent lines have the same or very similar slope, as detailed in Zhou *et al*. (2015b, c).

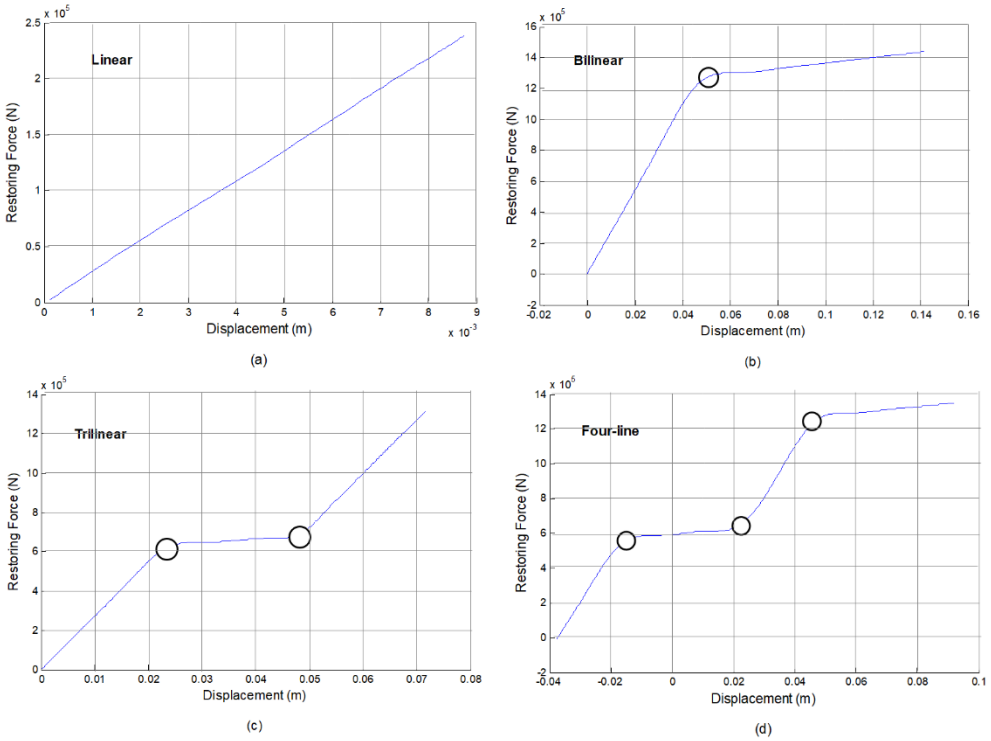

Fig. 4 Restoring force vs Displacement plots showing possible half-cycle responses for $\beta = 0.4$ with turning points indicated by circles, where: (a) is linear; (b) is a bilinear yielding half-cycle; (c) is trilinear and represents elastic loading, pinching, and subsequent elastic loading, typical of structures with $-1 < \beta < 0$; and (d) includes pinching response with $0 < \beta < 1$. All half-cycles shown are in tension, but will also occur in compression, but below the horizontal axis

2.4 Algorithm validation: *Simulated proof-of-concept structure*

The numerical proof-of-concept SDOF structure is a moment-resisting frame model of a five-story building, chosen for both realism and simplicity (Kao and Loh 2013). The seismic weight per floor is 1692 kN for roof level and 2067 kN for other levels. The building was designed using displacement-based design to sustain a target drift 2% under a 500-year return period earthquake. Fig. 5 shows the plan view and push-over analysis results for the proof-of-concept structure using Ruaumoko (Carr 2005). It shows a bilinear behaviour between base-shear and roof displacement with yield deformation of 46.5 mm, linear elastic stiffness of 27.3 kN/mm and a bilinear factor of 0.065. The estimated linear structural fundamental period is approximately 1.20 s.

A numerical model based on the flag-shaped model is used to simulate hysteresis and $f(x, \dot{x})$ in Eq. (1), for the proof-of-concept structure. In addition, 5% sensor noise is added for robustness in a Monte-Carlo analysis simulating all ground-motions (N = 20) and pinching factors (NN = 11 for β = -1, -0.8, -0.6 ... +1.0) combinations (N × NN = 220) 100 times for a total of 22,000 simulations. This Monte-Carlo analysis uses a random approximation of signal noise that varies randomly on each individual response analysis. This method of repeated simulation with varying noise values provides a range of possible outcomes to ensure that the results obtained and conclusions drawn are not specific to any individual result obtained from any one set of randomly-generated noise signals. The full set of 100 simulations with differing, randomly-generated, signal noise provides an indication of the range of potential outcomes, allowing consideration of the likelihood of different scenarios. While this method is relatively computationally intensive and requires 100 repetitions for each of the 220 sets of structural parameters, results can be considered with more confidence when such analyses are undertaken.

This Monte-Carlo analysis finds the variation in the identified plastic stiffness (k_p) over all plastic regimes of at least one-third the length of the longest plastic regime, with this threshold used to remove half cycles with negligible plastic deformation. A range of similar thresholds could be generated from pushover analysis.

2.5 Analyses

Table 1 shows the 20 ground motions used to test the robustness of the HLA algorithm to hysteresis loop shape. To test if the algorithm correctly identifies the (known) plastic regime stiffness of the structure for a range of ground motion frequency contents the identified plastic stiffness values are compared to the known ground truth. Measurements are assumed for displacement at 1 Hz and acceleration at 1 kHz. High frequency (1 kHz) displacement is obtained through double-integration and base-line correction using the low frequency (1 Hz) displacement measurement (Hann *et al.* 2009). Random 5% normally distributed noise is added to measurements used in the HLA algorithm to include this common source of error and

Table 1 Selected ground motions from PEER database (Peer 2005)

EQ	Event	Year	M_W	Station	R-Distance (km)	Soil type	Duration (s)	PGA (g)
EQ1	Superstition Hill	1987	6.7	Brawley	18.2	D	22.0	0.156
EQ2				EI Centro Imp. Co. Cent	13.9	D	40.0	0.358
EQ3				Plaster City	21.0	D	22.2	0.121
EQ4	Northridge	1994	6.7	Beverly Hills 14145 Muuhol	19.6	C	30.0	0.516
EQ5				Canoga Park – Topanga Can	15.8	D	25.0	0.356
EQ6				Glendale – Las Palmas	25.4	D	30.0	0.206
EQ7				LA – Hollywood Stor. FF	25.5	D	40.0	0.231
EQ8				N. Hollywood– Coldwater Can	14.6	C	21.9	0.273
EQ9				LA – N Faring Rd	23.9	D	30.0	0.298
EQ10				Sunland– Mt Gleason Ave	17.7	C	30.0	0.127
EQ11	Loma Prieta	1989	6.9	Capitola	14.5	D	40.0	0.529
EQ12				Gilroy Array #3	14.4	D	39.9	0.555
EQ13				Gilroy Array #4	16.1	D	40.0	0.417
EQ14				Gilroy Array #7	24.2	D	40.0	0.226
EQ15				Hollister Diff. Array	25.8	D	39.6	0.269
EQ16				Saratoga – W Valley Coll.	13.7	C	40.0	0.332
EQ17	Cape Mendocino	1992	7.1	Fortuna –Fortuna Blvd	23.6	C	44.0	0.116
EQ18				Rio Dell Overpass– FF	18.5	C	36.0	0.171
EQ19	Landers	1992	7.3	Desert Hot Springs	23.3	C	50.0	0.385
EQ20				Yermo Fire Station	24.9	D	44.0	0.245

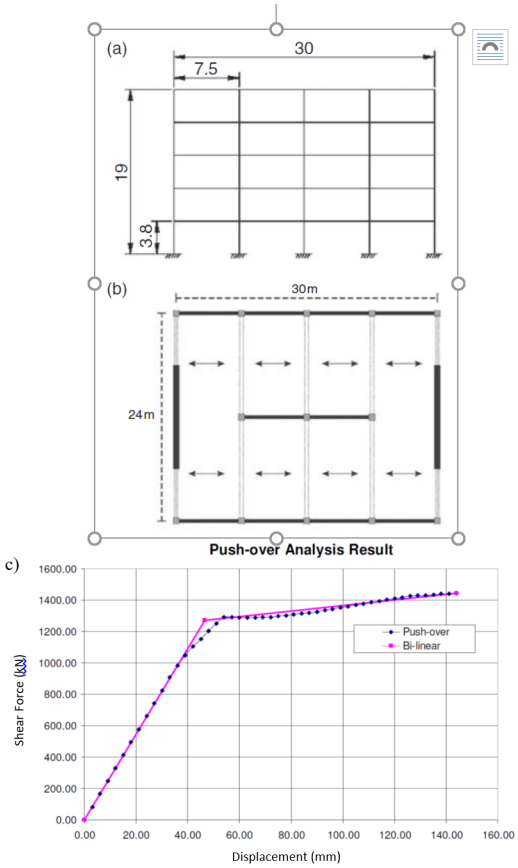

Fig. 5 Proof-of-concept numerical structure in (a) elevation; and (b) plan view; and (c) the result from the bilinear model and from pushover analysis result

account for errors up to ±15% (3 standard deviations). Monte Carlo analysis ensures a robust assessment of algorithm capability across all pinching factors, β.

Finally, a further sensitivity analysis on earthquake magnitude is run and repeats this Monte Carlo analysis for earthquakes with minimal plastic response to ensure the results are robust in the plastic regime across all events, and to further ensure ground motion selection is not causing erroneous or misleading results. In particular, these linear response ground motions are scaled from 1.0 (baseline) to 7.0 (extreme) to show where the identification for plastic stiffness converges where a largely or totally linear response will yield erroneous plastic stiffness identification.

3. Results and discussion

Table 2 shows the absolute percentage error between the identified plastic regime stiffness and the true (as-modelled) post yield stiffness of the simulated structure for a range of pinching factors and ground motion records. The Monte-Carlo analysis found the median (Inter-quartile range = IQR) absolute percentage error in k_p was 1.88% [0.79%, 4.94%].

There are notable exceptions to this accuracy in identifying k_p for Earthquakes 1, 6, 9 and 14 in Table 2. In these cases, larger error is explained by very minimal or negligible plastic deformation, creating an ill-defined k_p distribution where many, if not all, simulations do not provide a significant post-yield region to allow an accurate straight-line fit increasing the variability of identified k_p

Table 2 Table of percentage error in the median value of the reconstructed plastic regime stiffness for various pinching factors and simulated ground motions

		Pinching factor										
		-1	-0.8	-0.6	-0.4	-0.2	0	0.2	0.4	0.6	0.8	1
Ground motion number	1	100.00	100.00	100.00	100.00	100.00	100.00	100.00	100.00	100.00	100.00	100.00
	2	3.42	0.62	1.65	8.17	4.75	5.69	6.35	1.65	2.71	1.23	0.43
	3	7.23	30.30	95.66	194.28	245.97	7.23	7.23	7.23	91.40	13.27	4.65
	4	5.56	2.06	5.33	5.97	5.22	2.65	3.67	3.40	4.87	2.29	0.22
	5	2.58	6.25	2.71	4.95	2.89	2.82	3.14	5.60	5.23	1.82	1.21
	6	1412.21	1412.21	1412.21	1412.21	1412.21	1412.21	1412.21	1412.21	1412.21	1412.21	1412.21
	7	3.06	12.62	5.87	10.91	12.62	4.44	4.39	3.01	7.77	6.38	0.31
	8	2.14	3.35	5.70	5.94	4.76	2.07	4.57	3.53	4.59	2.97	0.35
	9	3248.96	3248.96	3248.96	3248.96	3248.96	3248.96	3248.96	3248.96	3248.96	3248.96	3248.96
	10	6381	10.13	109.00	228.46	6.81	6.81	6.80	6.81	237.90	122.89	14.68
	11	3.15	1.51	3.16	2.54	4.28	3.72	6.31	5.64	4.18	1.85	0.03
	12	32.98	32.98	29.04	26.74	22.29	20.41	32.98	11.15	41.32	50.08	115.43
	13	2.247	1.88	3.47	3.43	3.59	1.71	3.53	2.09	1.71	3.26	0.03
	14	549.05	549.05	549.05	549.05	549.05	549.05	549.05	549.05	549.05	549.05	549.05
	15	2.05	3.34	5.66	4.33	2.85	2.90	3.85	4.73	2.56	1.51	0.74
	16	1.88	4.26	2.67	1.80	2.19	1.99	4.22	4.12	2.15	1.89	0.50
	17	6.67	6.96	6.17	5.20	5.83	5.56	9.33	9.76	7.30	6.59	0.34
	18	2.74	4.59	6.78	6.58	7.01	3.22	4.23	3.32	3.22	2.03	0.23
	19	3.83	4.97	5.11	4.23	2.83	0.33	1.10	3.94	2.36	9.56	2.15
	20	2.23	2.41	5.75	3.09	6.76	1.11	3.84	3.98	2.80	2.79	0.09

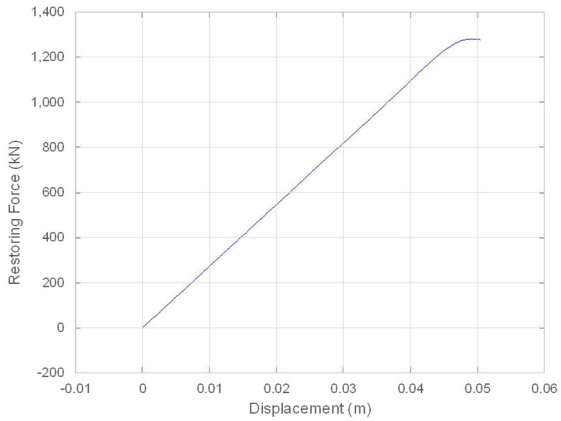

Fig. 6 A subsection with low levels of yielding, giving inaccurate identification of plastic regime stiffness from simulated response to earthquake 14 with pinching factor $\beta = 0.4$

values. This minimal plastic yielding is illustrated in Fig. 6, which shows a nonlinear half-cycle of response for Earthquake 14 with negligible plastic deformation using a pinching factor $\beta = 0.4$ and thus yielding an error of 549.05% in Table 2. The curved transition used in the forward simulation exacerbates this issue, but is more realistic than a sharper elastic-to-plastic transition.

Given the purpose of SHM is to indicate damage, it is not an issue for the algorithm to fail to clearly identify post-yield behaviour at such very low levels of yielding, since minor cumulative plastic deformation inflicts only minimal damage. However, to clarify this point, a sensitivity analysis on Earthquakes 1, 6, 9 and 14 performed by increasing their magnitude to increase plastic response. Fig. 7 shows the HLA algorithm would correctly identify the plastic regime stiffness as it converges to the true (lower dashed line) value as scaling factor increases. This result is also clear in the results for all other, larger earthquakes in Table 2, where the plastic response is larger and the identified plastic stiffness errors are far lower.

Finally, Fig. 8 shows the reconstructed hysteresis loop for Earthquake 6 with a scaling factor of 4 and pinching factor $\beta = 0.5$, to indicate plastic deformation only just starts to occur at this scaling factor, thus explaining the very high scaling needed for accurate identification with this particular seismic record. The overall Monte-Carlo analysis and this sensitivity analysis thus reveal the HLA algorithm is robust to sensor noise across all ground motion levels, when an appropriate threshold for negligible deformation is applied to eliminate spurious results.

The overall sensitivity analysis across pinching factors, earthquakes, and earthquake magnitude shows the HLA SHM algorithm is robust to ground motion frequency content, ground motion magnitude, measurement noise, and hysteresis loop shape presuming an appropriate threshold for negligible plastic deformation is used. This outcome is

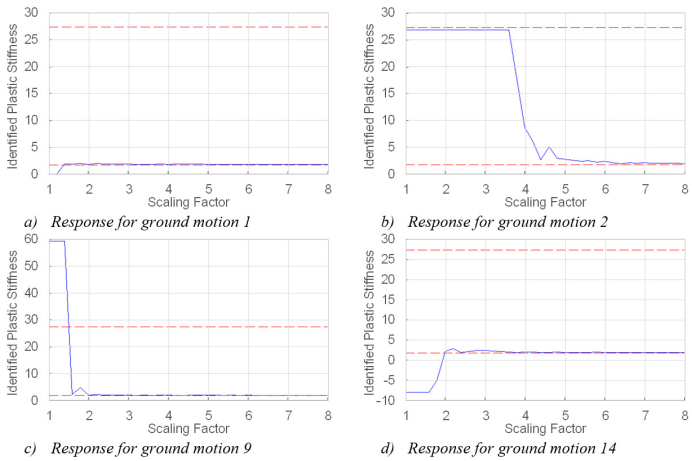

Fig. 7 Scaling factor sensitivity analysis for selected earthquake ground motions #1, 6, 9, and 14 which exhibit negligible plastic deformation results where the x-axis shows the ground motion scaling value from 1.0 (baseline) to 7.0 (extreme) and the resulting improved plastic stiffness value identification as more nonlinear response occurs with rising scale factor. The lower dashed line is the true plastic stiffness value. All identified stiffness values are given in kN/mm

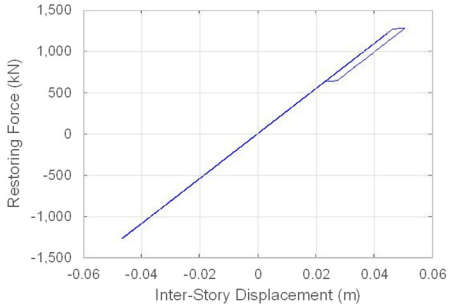

Fig. 8 Structural hysteresis loop for ground motion #6, with pinching factor $\beta = 0.5$, and scaling factor of 4 from Fig. 7(b)

particularly important since the actual hysteretic behaviour of a structure is not always readily estimated or expected due to ground motion frequency content, site-specific conditions, and/or construction errors. Thus, a generic algorithm that is not model-dependent can ensure correct identification of damage from permanent deformation and changes in k_e and/or k_p, where plastic stiffness evolution is not identified in most SHM algorithms.

This model-free hysteresis loop analysis approach thus offers potential advantages over the large number of model-based approaches, which require the overall response to broadly match the underlying baseline nonlinear mechanics model employed (Doebling *et al*. 1996, Zhou *et al*. 2017b, c, Xiong *et al*. 2019). Hence, it is more general and can manage a wide range of realistic hysteretic shapes, even within a given response, if it were to change behaviour.

However, this algorithm also has limitation to address. More specifically, incorrect identification of a turning point in a given half-cycle can cause high levels of elastic loading to be identified as plastic deformation, skewing the identified level of cumulative plastic deformation to be unrealistically large. It should be noted this limitation results in an inherently conservative outcome, where damage is over predicted, resulting in additional structural inspection required. This limitation was found to have a negligible effect on the performance of the algorithm in this analysis, as indicated by the high consistency shown in the Monte-Carlo analysis. However, the approach would benefit from more robust turning point identification with respect to sensor noise.

This analysis only examined a single degree of freedom case, assuming a typical first mode dominant seismic structural response (Chopra 1995, 2012). However, the measurement approach from (Toussi and Yao 1983, Iwan and Cifuentes 1986, Iemura and Jennings 1974) is readily and inexpensively extendable, as is the HLA method when considering real data (Zhou *et al*. 2015a, 2017a, b). Thus, one could obtain hysteresis loops story by story or for specific sets of stories, or sections within a more irregularly shaped structure. The overall approach presented would be equally applicable and robust using these more precisely located seismic hysteresis loop responses.

Further, the case study in this research is a regular structure and thus first mode dominant. However, HLA performs well on structures with other mode participation as has been demonstrated recently on real structural data (Rabiepour *et al*. 2022), and experimental work (Zhou *et al*. 2017a). However, this issue can also affect model-based SHM methods, as well, where the model identified may not match the actual response due to irregularity in design or construction (Zhou *et al*. 2017c). Finally, in the case of multiple higher modes, it is possible to use HLA effectively, either directly as it is stiffness and hysteresis loops used rather than a baseline model, or via a modal filtering approach (Poskus *et al*. 2020), although this latter approach provides added complexity.

4. Conclusions

This research analytically tests the robustness of the hysteresis loop analysis SHM method to a wide range of pinching nonlinear behaviours not typically examined in SHM methods due to their high nonlinearity. It further

focuses on tracking plastic stiffness values, which are not typically considered, but are a significant damage measure in their own right in assessing total plastic deformation and thus potential future failure due to low-cycle fatigue in any further larger aftershock or event. A Monte Carlo analysis on an analytical test case with known ground truth using 20 diverse ground motions, and including all sensor noise, for the full range of nonlinear pinching behaviours delivered 75% of errors in identifying plastic stiffness under 4.5%, where this limit declines to 3% when events generating no nonlinear behavior are removed. A sensitivity analysis on these events, increasing their magnitude to induce nonlinear behaviour, shows equally accurate identification when plastic behavior occurs. Overall, 95% of all errors were under 10%, ensuring the ability to accurately identify and track nonlinear stiffness value and its degradation, a novel capability in the field. Tracking these values over time during an event or a longer period enables more precise characterisation of structural degradation as well.

References

Adeli, H. and Jiang, X. (2006), "Dynamic fuzzy wavelet neural network model for structural system identification", *J. Struct. Eng.*, **132**, 102-111. DOI: 10.1061/(ASCE)0733-9445(2006)132:1(102)

Attanasi, G., Auricchio, F. and Fenves, G.L. (2009), "Feasibility assessment of an innovative isolation bearing system with shape memory alloys", *J. Earthq. Eng.*, **13**, 18-39. https://doi.org/10.1080/13632460902813216

Baber, T.T. and Noori, M.N. (1985), "Random vibration of degrading, pinching systems", *J. Eng. Mech.*, **111**, 1010-1026. https://doi.org/10.1061/(ASCE)0733-9399(1985)111:8(1010)

Bao, C., Hao, H. and Li, Z. (2013), "Vibration-based structural health monitoring of offshore pipelines: numerical and experimental study", *Struct. Control Health Monitor.*, **20**, 769-788. https://doi.org/10.1002/stc.1494

Bernal, D. and Gunes, B. (2000), "Observer/Kalman and subspace identification of the UBC benchmark structural model", *Proceedings of the 14th ASCE Engineering Mechanics Conference*, Austin, TX, USA, pp. 21-24.

Boore, D.M. and Bommer, J.J. (2005), "Processing of strong-motion accelerograms: needs, options and consequences", *Soil Dyn. Earthq. Eng.*, **25**, 93-115. https://doi.org/10.1016/j.soildyn.2004.10.007

Brownjohn, J.M. (2007), "Structural health monitoring of civil infrastructure", *Philosoph. Transact. Royal Soc. A: Mathe. Phys. Eng. Sci.*, **365**, 589-622. https://doi.org/10.1098/rsta.2006.1925

Brownjohn, J.M.W., Raby, A., Au, S.-K., Zhu, Z., Wang, X., Antonini, A., Pappas, A. and D'ayala, D. (2019), "Bayesian operational modal analysis of offshore rock lighthouses: Close modes, alignment, symmetry and uncertainty", *Mech. Syst. Signal Process.*, **133**, 106306. https://doi.org/10.1016/j.ymssp.2019.106306

Carr, A.J. (2005), RUAUMOKO program for inelastic dynamic analysis: user manual, Department of Civil Engineering, University of Canterbury, Christchurch, New Zealand.

Chang, P.C., Flatau, A. and Liu, S. (2003), "Health monitoring of civil infrastructure", *Struct. Health Monitor.*, **2**, 257-267. https://doi.org/10.1177/1475921703036169

Chase, J.G., Hwang, K.L., Barroso, L.R. and Mander, J.B. (2005), "A simple LMS-based approach to the structural health monitoring benchmark problem", *Earthq. Eng. Struct. Dyn.*, **34**, 575-594. https://doi.org/10.1002/eqe.433

Chen, B., Zhao, S.-L. and Li, P.-Y. (2014), "Application of Hilbert-Huang transform in structural health monitoring: a state-of-the-art review", *Mathe. Problems Eng.*, 2014. https://doi.org/10.1155/2014/317954

Chopra, A.K. (1995), *Dynamics of Structures: Theory and Applications to Earthquake Engineering*, Prentice Hall, Upper Saddle River, NJ, USA.

Chopra, A.K. (2012), *Dynamics of Structures*, Pearson Education Upper Saddle River, NJ, USA.

Christopoulos, C., Filiatrault, A. and Folz, B. (2002), "Seismic response of self-centring hysteretic SDOF systems", *Earthq. Eng. Struct. Dyn.*, **31**, 1131-1150. https://doi.org/10.1002/eqe.152

Christopoulos, C., Pampanin, S. and Nigel Priestley, M. (2003), "Performance-based seismic response of frame structures including residual deformations part I: single-degree of freedom systems", *J. Earthq. Eng.*, **7**, 97-118. https://doi.org/10.1142/S1363246903000894

Christopoulos, C., Tremblay, R., Kim, H.-J. and Lacerte, M. (2008), "Self-centering energy dissipative bracing system for the seismic resistance of structures: development and validation", *J. Struct. Eng.*, **134**, 96-107. https://doi.org/10.1061/(ASCE)0733-9445(2008)134:1(96)

De Lautour, O.R. and Omenzetter, P. (2010), "Damage classification and estimation in experimental structures using time series analysis and pattern recognition", *Mech. Syst. Signal Process.*, **24**, 1556-1569. https://doi.org/10.1016/j.ymssp.2009.12.008

Doebling, S.W., Farrar, C.R., Prime, M.B. and Shevitz, D.W. (1996), "Damage identification and health monitoring of structural and mechanical systems from changes in their vibration characteristics: a literature review", Los Alamos National Lab., NM, USA.

Doherty, J.E. (1987), "Non-destructive evaluation", In: Kobayashi, A.S. (ed.), *Handbook on Experimental Mechanics*, (1st ed.) Prentice-Hall, Inc., Englewood Cliffs, NJ, USA.

Fan, W. and Qiao, P. (2011), "Vibration-based damage identification methods: a review and comparative study", *Struct. Health Monitor.*, **10**, 83-111. https://doi.org/10.1177/1475921710365419

Favvata, M.J. and Karayannis, C.G. (2014), "Influence of pinching effect of exterior joints on the seismic behavior of RC frames", *Earthq. Struct., Int. J.*, **6**(1), 89-110. https://doi.org/10.12989/eas.2014.6.1.089

Feng, D. and Feng, M.Q. (2017), "Identification of structural stiffness and excitation forces in time domain using noncontact vision-based displacement measurement", *J. Sound Vib.*, **406**, 15-28. https://doi.org/10.1016/j.jsv.2017.06.008

Feng, D. and Feng, M.Q. (2018), "Computer vision for SHM of civil infrastructure: From dynamic response measurement to damage detection–A review", *Eng. Struct.*, **156**, 105-117. https://doi.org/10.1016/j.engstruct.2017.11.018

Foliente, G.C. and Noori, M.N. (1996), "Equivalent linearization of generally pinching hysteretic, degrading systems", *Earthq. Eng. Struct. Dyn.*, **25**, 611-629. https://doi.org/10.1002/(SICI)1096-9845(199606)25:6<611::AID-EQE572>3.0.CO;2-S

Ginsberg, D., Fritzen, C.-P. and Loffeld, O. (2018), "Sparsity-constrained extended Kalman filter concept for damage localization and identification in mechanical structures", *Smart Struct. Syst., Int. J.*, **21**(6), 741-749. https://doi.org/10.12989/sss.2018.21.6.741

Hann, C.E., Singh-Levett, I., Deam, B.L., Mander, J.B. and Chase, J.G. (2009), "Real-time system identification of a nonlinear four-story steel frame structure—application to structural health monitoring", *IEEE Sensors J.*, **9**, 1339-1346. https://doi.org/10.1109/JSEN.2009.2022434

Hannan, M.A., Hassan, K. and Jern, K.P. (2018), "A review on sensors and systems in structural health monitoring: current issues and challenges", *Smart Struct. Syst.*, *Int. J.*, **22**(5), 509-525. https://doi.org/10.12989/sss.2018.22.5.509

Hou, Z., Noori, M. and Amand, R.S. (2000), "Wavelet-based approach for structural damage detection", *J. Eng. Mech.*, **126**, 677-683. https://doi.org/10.1061/(ASCE)0733-9399(2000)126:7(677)

Hou, Z., Hera, A. and Shinde, A. (2006), "Wavelet-based structural health monitoring of earthquake excited structures. Computer-Aided Civil and Infrastructure Engineering, 21, 268-279.

Huang, Q.D., Gardoni, P. and Hurlebaus, S. (2012), "A probabilistic damage detection approach using vibration-based nondestructive testing", *Struct. Safety*, **38**, 11-21. https://doi.org/10.1016/j.strusafe.2012.01.004

Hung, S.L., Huang, C., Wen, C. and Hsu, Y. (2003), "Nonparametric identification of a building structure from experimental data using wavelet neural network", *Comput.-Aided Civil Infrastr. Eng.*, **18**, 356-368. https://doi.org/10.1111/1467-8667.t01-1-00313

Iemura, H. and Jennings, P. (1974), "Hysteretic response of a nine-storey reinforced concrete building", *Earthq. Eng. Struct. Dyn.*, **3**, 183-201. https://doi.org/10.1002/eqe.4290030207

Iwan, W.D. and Cifuentes, A.O. (1986), "A model for system identification of degrading structures", *Earthq. Eng. Struct. Dyn.*, **14**, 877-890. https://doi.org/10.1002/eqe.4290140605

Jeen-Shang, L. and Yigong, Z. (1994), "Nonlinear structural identification using extended Kalman filter", *Comput. Struct.*, **52**, 757-764. https://doi.org/10.1016/0045-7949(94)90357-3

Jesus, A., Brommer, P., Westgate, R., Koo, K., Brownjohn, J. and Laory, I. (2019), "Modular Bayesian damage detection for complex civil infrastructure", *J. Civil Struct. Health Monitor.*, **9**, 201-215. https://doi.org/10.1007/s13349-018-00321-8

Jiang, X. and Adeli, H. (2005), "Dynamic wavelet neural network for nonlinear identification of highrise buildings", *Comput.-Aided Civil Infrastr. Eng.*, **20**, 316-330. https://doi.org/10.1111/j.1467-8667.2005.00399.x

Kao, C.Y. and Loh, C.H. (2013), "Monitoring of long-term static deformation data of Fei-Tsui arch dam using artificial neural network-based approaches", *Struct. Control Health Monitor.*, **20**, 282-303. https://doi.org/10.1002/stc.492

Kunnath, S.K., Mander, J.B. and Fang, L. (1997), "Parameter identification for degrading and pinched hysteretic structural concrete systems", *Eng. Struct.*, **19**, 224-232. https://doi.org/10.1016/S0141-0296(96)00058-2

Kunwar, A., Jha, R., Whelan, M. and Janoyan, K. (2013), "Damage detection in an experimental bridge model using Hilbert–Huang transform of transient vibrations", *Struct. Control Health Monitor.*, **20**, 1-15. https://doi.org/10.1002/stc.466

Lin, S., Yang, J.N. and Zhou, L. (2005), "Damage identification of a benchmark building for structural health monitoring", *Smart Mater. Struct.*, **14**, S162. https://doi.org/10.1088/0964-1726/14/3/019

Loh, C.-H., Lin, C.-Y. and Huang, C.-C. (2000), "Time domain identification of frames under earthquake loadings", *J. Eng. Mech.*, **126**, 693-703. https://doi.org/10.1061/(ASCE)0733-9399(2000)126:7(693)

Nayyerloo, M., Chase, J., Macrae, G. and Chen, X. (2011), "LMS-based approach to structural health monitoring of nonlinear hysteretic structures", *Struct. Health Monitor.*, **10**, 429-444. https://doi.org/10.1177/1475921710379519

Ozbulut, O.E. and Hurlebaus, S. (2010), "Seismic assessment of bridge structures isolated by a shape memory alloy/rubber-based isolation system", *Smart Mater. Struct.*, **20**, 015003. https://doi.org/10.1088/0964-1726/20/1/015003

Pampanin, S., Christopoulos, C. and Nigel Priestley, M. (2003), "Performance-based seismic response of frame structures including residual deformations part II: multi-degree of freedom systems", *J. Earthq. Eng.*, **7**, 119-147. https://doi.org/10.1142/S1363246903000900

Pan, S., Xiao, D., Xing, S., Law, S., Du, P. and Li, Y. (2016), "A general extended Kalman filter for simultaneous estimation of system and unknown inputs", *Eng. Struct.*, **109**, 85-98. https://doi.org/10.1016/j.engstruct.2015.11.014

Park, S., Park, H.S., Kim, J. and Adeli, H. (2015), "3D displacement measurement model for health monitoring of structures using a motion capture system", *Measurement*, **59**, 352-362. https://doi.org/10.1016/j.measurement.2014.09.063

Peer (2005), "Pacific Earthquake Engineering Research Center (PEER) Strong Motion Database [Online], Pacific Earthquake Engineering Research Center, CA, USA. Available: https://peer.berkeley.edu/peer-strong-ground-motion-databases [Accessed January 5 2021]

Pines, D. and Salvino, L. (2006), "Structural health monitoring using empirical mode decomposition and the Hilbert phase", *J. Sound Vib.*, **294**, 97-124. https://doi.org/10.1016/j.jsv.2005.10.024

Poskus, E., Rodgers, G.W. and Chase, J.G. (2020), "Output-only modal parameter identification of systems subjected to various types of excitation", *J. Eng. Mech.*, **146**, 04020129. https://doi.org/10.1061/(ASCE)EM.1943-7889.0001853

Rabiepour, M., Zhou, C., Rodgers, G.W. and Chase, J.G. (2022), "Real-world application of hysteresis loop analysis for stiffness identification of an instrumented building across multiple seismic events", *J. Build. Eng.*, **45**, 103524. https://doi.org/10.1016/j.jobe.2021.103524

Rodgers, G., Solberg, K., Chase, J., Mander, J., Bradley, B., Dhakal, R. and Li, L. (2008), "Performance of a damage-protected beam–column subassembly utilizing external HF2V energy dissipation devices", *Earthquake Engineering & Structural Dynamics* (*EESD*), **37**, 1549-1564. https://doi.org/10.1002/eqe.830

Rodgers, G.W., Mander, J.B. and Chase, J.G. (2011), "Semi-explicit rate-dependent modeling of damage-avoidance steel connections using HF2V damping devices", *Earthq. Eng. Struct. Dyn.*, **40**, 977-992. https://doi.org/10.1002/eqe.1073

Rodgers, G.W., Solberg, K.M., Mander, J.B., Chase, J.G., Bradley, B.A. and Dhakal, R.P. (2012), "High-force-to-volume seismic dissipators embedded in a jointed precast concrete frame", *J. Struct. Eng.*, **138**, 375-386. https://doi.org/10.1061/(ASCE)ST.1943-541X.0000329

Sato, T. and Qi, K. (1998), "Adaptive H∞ filter: Its application to structural identification", *J. Eng. Mech.*, **124**, 1233-1240. https://doi.org/10.1061/(ASCE)0733-9399(1998)124:11(1233)

Sivaselvan, M.V. and Reinhorn, A.M. (2000), "Hysteretic models for deteriorating inelastic structures", *J. Eng. Mech.*, **126**, 633-640. https://doi.org/10.1061/(ASCE)0733-9399(2000)126:6(633)

Skolnik, D.A. and Wallace, J.W. (2010), "Critical assessment of interstory drift measurements", *J. Struct. Eng.*, **136**, 1574-1584. https://doi.org/10.1061/(ASCE)ST.1943-541X.0000255

Sohn, H., Farrar, C.R., Hemez, F.M., Shunk, D.D., Stinemates, D.W., Nadler, B.R. and Czarnecki, J.J. (2004), "A Review of Structural Health Monitoring Literature: 1996-2001", Los Alamos National Laboratory.

Stephens, J.E. and Yao, J.T. (1987), "Damage assessment using response measurements", *J. Struct. Eng.*, **113**, 787-801. https://doi.org/10.1061/(ASCE)0733-9445(1987)113:4(787)

Sun, K., Zhang, W., Ding, H., Kim, R.E. and Spencer, B.F. (2017), "Autonomous evaluation of ambient vibration of underground spaces induced by adjacent subway trains using high-sensitivity wireless smart sensors", *Smart Struct. Syst.*, *Int. J.*, **19**(1), 1-10.

https://doi.org/10.12989/sss.2017.19.1.001

Taha, M.R., Noureldin, A., Lucero, J. and Baca, T. (2006), "Wavelet transform for structural health monitoring: a compendium of uses and features", *Struct. Health Monitor.*, **5**, 267-295. https://doi.org/10.1177/1475921706067741

Toussi, S. and Yao, J.T. (1983), "Hysteresis identification of existing structures", *J. Eng. Mech.*, **109**, 1189-1202. https://doi.org/10.1061/(ASCE)0733-9399(1983)109:5(1189)

Tremblay, R., Lacerte, M. and Christopoulos, C. (2008), "Seismic response of multistory buildings with self-centering energy dissipative steel braces", *J. Struct. Eng.*, **134**, 108-120. https://doi.org/10.1061/(ASCE)0733-9445(2008)134:1(108)

Vamvatsikos, D. and Cornell, C.A. (2002), "Incremental dynamic analysis", *Earthq. Eng. Struct. Dyn.*, **31**, 491-514. https://doi.org/10.1002/eqe.141

Wen, Y.-K. (1976), "Method for random vibration of hysteretic systems", *J. Eng. Mech. Div.*, **102**, 249-263. https://doi.org/10.1061/JMCEA3.0002106

Wrzesniak, D., Rodgers, G.W., Fragiacomo, M. and Chase, J.G. (2016), "Experimental testing of damage-resistant rocking glulam walls with lead extrusion dampers", *Constr. Build. Mater.*, **102**, 1145-1153. https://doi.org/10.1016/j.conbuildmat.2015.09.011

Wu, M. and Smyth, A. (2008), "Real-time parameter estimation for degrading and pinching hysteretic models", *Int. J. Non-Linear Mech.*, **43**, 822-833. https://doi.org/10.1016/j.ijnonlinmec.2008.05.010

Wu, Z., Xu, B. and Yokoyama, K. (2002), "Decentralized parametric damage detection based on neural networks", *Comput.-Aided Civil Infrastr. Eng.*, **17**, 175-184. https://doi.org/10.1111/1467-8667.00265

Xiong, H.-B., Cao, J.-X., Zhang, F.-L., Ou, X. and Chen, C.-J. (2019), "Investigation of the SHM-oriented model and dynamic characteristics of a super-tall building", *Smart Struct. Syst., Int. J.*, **23**(3), 295-306. https://doi.org/10.12989/sss.2019.23.3.295

Xu, Y. and Brownjohn, J.M. (2018), "Review of machine-vision based methodologies for displacement measurement in civil structures", *J. Civil Struct. Health Monitor.*, **8**, 91-110. https://doi.org/10.1007/s13349-017-0261-4

Xu, C., Chase, J.G. and Rodgers, G.W. (2014), "Physical parameter identification of nonlinear base-isolated buildings using seismic response data", *Comput. Struct.*, **145**, 47-57. https://doi.org/10.1016/j.compstruc.2014.08.006

Yang, J.N., Lei, Y., Lin, S. and Huang, N. (2004), "Hilbert-Huang based approach for structural damage detection", *J. Eng. Mech.*, **130**, 85-95. https://doi.org/10.1061/(ASCE)0733-9399(2004)130:1(85)

Yang, J.N., Lin, S., Huang, H. and Zhou, L. (2006), "An adaptive extended Kalman filter for structural damage identification", *Struct. Control Health Monitor.*, **13**, 849-867. https://doi.org/10.1002/stc.84

Yang, J., Pan, S. and Huang, H. (2007), "An adaptive extended Kalman filter for structural damage identifications II: unknown inputs", *Struct. Control Health Monitor.*, **14**, 497-521. https://doi.org/10.1002/stc.171

Yang, J.N., Xia, Y. and Loh, C.-H. (2014), "Damage detection of hysteretic structures with a pinching effect", *J. Eng. Mech.*, **140**, 462-472. https://doi.org/10.1061/(ASCE)EM.1943-7889.0000581

Ye, X., Su, Y. and Han, J. (2014), "Structural health monitoring of civil infrastructure using optical fiber sensing technology: A comprehensive review", *Scient. World J.*, 2014. https://doi.org/10.1155/2014/652329

Ye, X., Yi, T.-H., Dong, C., Liu, T. and Bai, H. (2015), "Multi-point displacement monitoring of bridges using a vision-based approach", *Wind Struct., Int. J.*, **20**(2), 315-326. https://doi.org/10.12989/was.2015.20.2.315

Ye, X., Yi, T.-H., Su, Y., Liu, T. and Chen, B. (2017), "Strain-based structural condition assessment of an instrumented arch bridge using FBG monitoring data", *Smart Struct. Syst., Int. J.*, **20**(2), 139-150. https://doi.org/10.12989/sss.2017.20.2.139

Ye, X., Jin, T. and Yun, C. (2019), "A review on deep learning-based structural health monitoring of civil infrastructures", *Smart Struct. Syst., Int. J.*, **24**(5), 567-585. https://doi.org/10.12989/sss.2019.24.5.567

Yu, J., Yu, K., Shang, X. and Lu, Z. (2016), "New Extended Finite Element Method for Pinching Effect in Reinforced Concrete Columns", *ACI Struct. J.*, **113**(4), 689-699.

Zhou, C., Chase, J.G., Rodgers, G.W., Kuang, A., Gutschmidt, S. and Xu, C. (2015a), "Performance evaluation of CWH base isolated building during two major earthquakes in Christchurch", *Bull. New Zealand Soc. Earthq. Eng.*, **48**, 264-273. https://doi.org/10.5459/bnzsee.48.4.264-273

Zhou, C., Chase, J.G., Rodgers, G.W., Tomlinson, H. and Xu, C. (2015b), "Physical parameter identification of structural systems with hysteretic pinching", *Comput.-Aided Civil Infrastr. Eng.*, **30**, 247-262. https://doi.org/10.1111/mice.12108

Zhou, C., Chase, J.G., Rodgers, G.W., Xu, C. and Tomlinson, H. (2015c), "Overall damage identification of flag-shaped hysteresis systems under seismic excitation", *Smart Struct. Syst., Int. J.*, **16**(1), 163-181. https://doi.org/10.12989/sss.2015.16.1.163

Zhou, C., Chase, J.G. and Rodgers, G.W. (2017a), "Efficient hysteresis loop analysis-based damage identification of a reinforced concrete frame structure over multiple events", *J. Civil Struct. Health Monitor.*, **7**, 541-556. https://doi.org/10.1007/s13349-017-0241-8

Zhou, C., Chase, J.G., Rodgers, G.W. and Iihoshi, C. (2017b), "Damage assessment by stiffness identification for a full-scale three-story steel moment resisting frame building subjected to a sequence of earthquake excitations", *Bull. Earthq. Eng.*, **15**, 5393-5412. https://doi.org/10.1007/s10518-017-0190-y

Zhou, C., Chase, J.G., Rodgers, G.W. and Xu, C. (2017c), "Comparing model-based adaptive LMS filters and a model-free hysteresis loop analysis method for structural health monitoring", *Mech. Syst. Signal Process.*, **84**, 384-398. https://doi.org/10.1016/j.ymssp.2016.07.030

CC